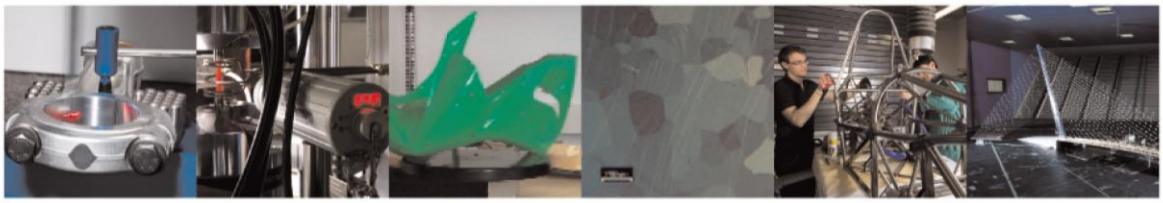

Influence of pulsed and continuous wave emission on melting efficiency in selective laser melting

Caprio, Leonardo; Demir, Ali Gökhan; Previtali, Barbara

This is a post-peer-review, pre-copyedit version of an article published in JOURNAL OF MATERIALS PROCESSING TECHNOLOGY. The final authenticated version is available online at: http://dx.doi.org/10.1016/j.jmatprotec.2018.11.019

DIPARTIMENTO DI MECCANICA ■ POLITECNICO DI MILANO
via G. La Masa, 1 ■ 20156 Milano ■ EMAIL (PEC): pecmecc@cert.polimi.it
http://www.mecc.polimi.it
Rev. 0

Influence of pulsed and continuous wave emission on melting efficiency in selective laser melting

Leonardo Caprio*, Ali Gökhan Demir, Barbara Previtali

Department of Mechanical Engineering, Politecnico di Milano, Via La Masa 1, 20156 Milan, Italy

*Corresponding author: leonardo.caprio@polimi.it

List of symbols

Symbol	Name	Units
N_{layers}	Number of layers of deposited material	non-dimensional
N_p	Number of pulses in one single track	non-dimensional
P_{avg}	Average output power	W
P_{back}	Pulse background power	W
P_{pk}	Pulse peak power	W
T_0	Room temperature	°C
c_p	Specific heat capacity	$Jkg^{-1}K^{-1}$
d_0	Beam waist diameter	m
k_s	Bulk solid thermal conductivity	$Wm^{-1}K^{-1}$
k_s	Powder bed thermal conductivity	$Wm^{-1}K^{-1}$
r_B	Gaussian distribution parameter (for 1/*e)*	m
t_0	Time constant	s
t_{off}	Laser off period	s
t_{on}	Pulse duration	s
t_{tot}	Pulsation period	s
v_{cw}	Scanning speed with CW emission	ms^{-1}
v_{cwEQ}	Equivalent scanning speed	ms^{-1}
v_{pw}	Scanning speed with PW emission	ms^{-1}
w_{melt}	Simulated track width	µm
α_s	Bulk solid thermal diffusivity	m^2s^{-1}
α_p	Powder bed solid thermal diffusivity	m^2s^{-1}
ρ_s	Bulk solid density	kgm^{-3}
ρ_p	Powder bed solid density	kgm^{-3}
ΔT_b	Temperature increase by pulse background power	°C
ΔT_p	Temperature increase by pulse peak power	°C
BR	Build rate	cm^3h^{-1}
M	Integration constant n°1	non-dimensional

N	Integration constant n°2	non-dimensional
P	Integration constant n°3	non-dimensional
PRR	Pulse repetition rate	Hz
V	Volume of deposited material	mm^3
a	Integral limit n°1	non-dimensional
b	Integral limit n°2	non-dimensional
l	Length of a single track	m
l_t	Layer thickness	µm
n	n-th pulse	non-dimensional
v	Speed of moving heat source	ms^{-1}
w	Mean track width	µm
x, y, z	Absolute coordinate system	m
δ	Duty cycle	non-dimensional
η	Process efficiency	non-dimensional
θ	Relative density	non-dimensional
μ	Integration variable	non-dimensional
ξ	Relative coordinate system	m

Graphical Abstract

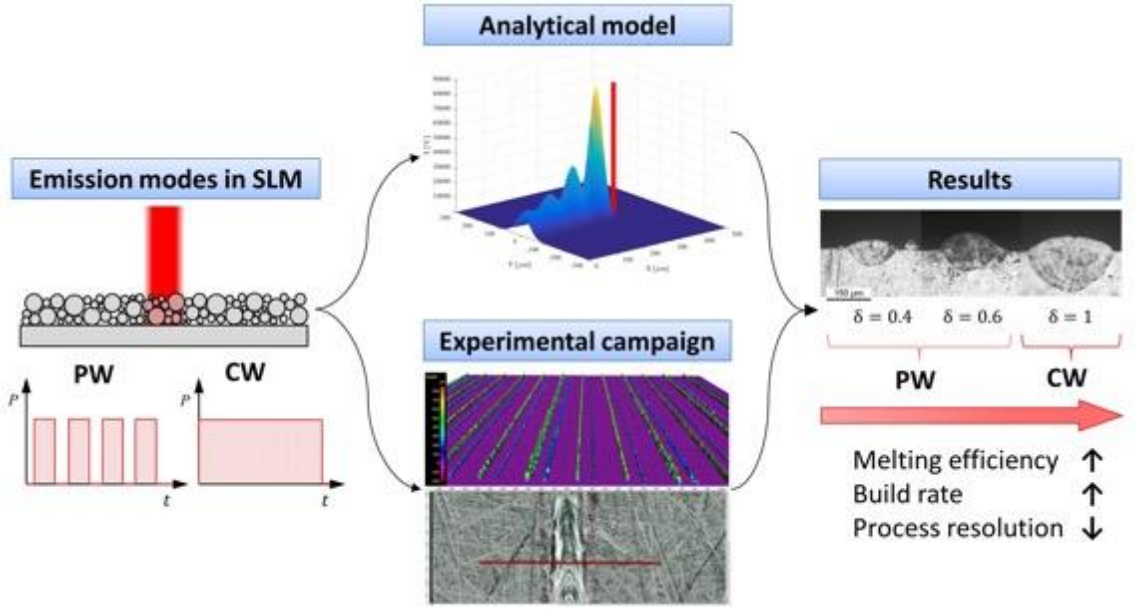

Abstract

A wide proportion of the industrial Selective Laser Melting (SLM) systems are operated with high brilliance fiber laser sources. These sources are most commonly operated in continuous wave (CW). A smaller fraction of these systems employs pulsed wave (PW) emission by power modulation, resulting in pulses with µs level durations, kHz level repetition rates and comparable peak powers to CW emission. Clearly, the laser temporal emission mode can have an impact over temperature fields, which in return control the melt pool size, stability and densification behaviour. The aim of this paper is to investigate the effect of laser emission regime on the melting efficiency in SLM. In particular, an analytical model was developed to investigate the process efficiency in single track formation at fixed energy input when employing different emission modes. A single mode fiber laser installed on an in-house developed prototype powder bed fusion system was used as the experimental setup with AISI 316L metallic powders. The effect of duty cycle was evaluated starting from CW (i.e. 100% duty) moving towards PW, at fixed energy density levels. Results show that at constant energetic input, CW increases process melting efficiency up to 3 times whilst the deposition stability is reduced with lower duty in PW regime. Although less efficient, at stable conditions the use of modulated emission produces narrower tracks providing higher process resolution.

Keywords: selective laser melting; AISI 316L; melting efficiency; emission mode; analytical model

1. Introduction

In the current industrial panorama, additive manufacturing technologies are beginning an alternative to conventional methods of production. Amongst these, Selective Laser Melting has attested itself as capable of moving from rapid prototyping applications to full scale production of high value mechanical components. This is demonstrated in the biomedical components realised by Santos et al. (2006) as well as the numerous applications which have been reviewed by Yap et al. (2015), ranging from heat exchangers to dental applications and jewellery. Nonetheless, many challenges yet remain open towards obtaining a greater process control to optimise mechanical behaviour and geometrical accuracy of SLM processed parts. In particular, densification behaviour of the powder bed has been identified as key aspects that control part quality. For instance, Mumtaz and Hopkinson (2009) investigated the effect of emission parameters on the top and surface roughness of IN625 thin walled structures. Analogously, Demir et al. (2017) showed the effect of different processing conditions on part accuracy and density of 18Ni300 maraging steel test geometries. Panwisawas et al. (2015) demonstrated through modelling and experimental results the role of thermodynamics in the formation of part porosity of Ti6Al4V samples. In their comprehensive work on a methodological approach for process parameter development, Yadroitsev et al. (2015) demonstrate the importance of fundamental studies for the successful identification of optimal processing conditions. Therefore, a greater understanding of the basic phenomena occurring during the powder bed fusion process is of interest for the scientific community.

Control over the temporal profile of the laser power delivered to the material has been identified as a highly influencing aspect on thermal processes analogous to Selective Laser Melting. The work by Kuo and Lin (2007) stands out as highly significative in comparing pulsed wave (PW) and continuous wave (CW) emission for the laser welding of a Ni-based superalloy as well as the research by Assuncao and Williams (2013) for mild steel joining. Kuo and Lin (2007) indicate that PW emission

might be detrimental for porosity formation due to lower melt pool stability, whilst Assuncao and Williams (2013) identify a difference in the transition from conduction mode welding to keyholing. Both works were conducted using PW emission with higher peak powers with respect to CW emission.

To the present date, the greater part of industrial SLM systems uses high brilliance fiber laser sources with continuous wave emission whereas only some employ fast power modulation of the diode pumping current, generating pulsed wave emission with peak powers comparable to CW emission (also denoted as modulated emission). The choice in terms of emission modes by system manufacturers was previously reviewed by Demir et al. (2017) and Biffi et al. (2018) and shows that EOS GmbH, Trumpf GmbH, Concept Laser GmbH, SLM Solutions GmbH, Realizer GmbH and Sisma SpA for instance prefer continuous power delivery whereas only Renishaw plc adopts modulated emission. However, part quality indicators of the SLM process such as porosity, thermal stresses, dimensional accuracy and surface roughness are yet to be investigated with different emission modes. In literature there is evidence that PW emission can have beneficial effects in minimising thermal distortions and increasing process resolution thanks to a more contained melt pool formation as demonstrated by Mumtaz and Hopkinson (2009, 2010). Moreover, the tailoring of process parameters might enable the realisation of finer features as shown by Demir and Previtali (2017) for the additive manufacturing of cardiovascular stents. From a microstructural perspective, Biffi et al. (2018) examined the properties of AlSi10Mg samples produced with CW and modulated emission on different commercial machines. Their results show that continuous wave emission dictates a greater precipitation of Mg_2Si, whilst more lattice defects could be identified in the samples deposited with PW emission. This different behaviour is related by Biffi et al. (2018) to the thermal history of the material. However, no authors have yet investigated this theme from a fundamental perspective and will therefore be the aim of the present work.

With regards to the study of the principles of metal powder densification in the SLM technology, single track studies have often been conducted. Li et al. (2012) have used this methodology to understand the balling defect formation, Aboulkhair et al. (2016) to study the porosity formation mechanisms in the deposition of AlSi10Mg. On the other hand, Averyanova et al. (2012) used an experimental design approach to identify the correct processing conditions for the deposition of 17-4 PH martensitic steel, Ciurana et al. (2013) to optimise process parameters for the SLM of CoCrMo alloy whilst Zhang and Coddet (2015) investigated the deposition of pure Fe. Extensive experimentation on single track formation of different alloys was also conducted by Yadroitsev et al. (2007). In particular, the research by Yadroitsev et al. (2009, 2013) was aimed at determining process feasibility zones (of stable and unstable deposition) processing parameters for the realisation of fine structured components. More recently, the track densification and process dynamics have been observed with high speed imaging techniques showing the influence of process parameters on the melt pool solidification as well as gas dynamics and beam spatial profile. In particular, Bidare et al. (2017, 2018) investigated both melt flow and gas flow dynamics through high speed imaging of single track deposition. Using an analogous approach Scipioni Bertoli et al. (2017), measured cooling rates of the laser powder bed fusion process at varying levels of process parameters, whilst Trapp et al. (2017) conducted in-situ absorptivity measurements. Furthermore, using single track deposition studies Roehling et al. (2017) showed how spatial beam shaping of the laser beam can aid in controlling the microstructural evolution of the powder bed fusion process. A common feature of these recent attempts is the use of customized equipment in order to flexibly control the processing conditions, which is not commonly possible with industrial systems.

Therefore, in the present work it was chosen to investigate the effect of temporal modulation of the laser input on the process efficiency using a similar approach. The realisation of single tracks was conducted using a flexible in-house developed SLM prototype system. Experimental results from the

present investigation show that at single track deposition level, with varying levels of duty cycle and delivered energy, significant differences appear in the volume of solidified material and track width. These aspects are fundamental in determining build rate and process resolution for SLM.

Accordingly, the understanding of the physics of a process must be achieved through its modelling and in the literature of laser material processing, the interaction between laser beams and workpiece material has often modelled as a purely thermal phenomenon as in the research on heat treatment by Ashby and Easterling (1984) or Cline and Anthony (1977) and on the laser welding process by Eagar and Tsai (1983). Currently, the greater part of the research efforts regarding the modelling of the SLM process have been directed towards numerical solutions as clearly shown in the literature review by Zeng et al. (2012). Nonetheless, this approach requires elevated computational times and an elevated number of input variable which do not allow for the understanding of the physics underlying in a process. Analytical models are effective in summarising the effect of the principal input parameters although their limitations reside in the strong hypotheses. Still, in the laser material processing field there is extensive evidence of the use of analytical solutions to investigate heat transfer mechanisms, as in the examples previously mentioned but also in numerous others: for instance Gellert and Egli (1988) modelled the pulsed laser melting of copper using a motionless heat source model, Steen et al. (1988) modelled the keyhole laser welding through a superposition of the point and line heat sources. Ducharme et al. (1994) analogously employed a moving heat source model to predict weld pool shapes and Binda et al. (2004) adopted a semi-empirical solution to determine the weld beads for AISI 304.

The aim of this work is to assess the efficiency of the pulsed and continuous wave emission modes using a semi-analytical approach. An analytical model which takes into account the main spatial and temporal parameters affecting the energy delivered to the powder bed during the SLM processing of

single tracks is developed. The model is used to identify changes in the process efficiency related to duty cycle, which is the main parameter defining the temporal emission profile.

The present research is structured in two main sections: the first presenting the experimental results of a campaign comparing continuous wave and pulsed wave emission; the second studying the variations of the heat transfer efficiency of the SLM process in the different experimental conditions, explaining the variations in the densification behaviour. Results confirm that process efficiency is up to three times greater with CW emission compared to PW emission.

2. Modelling of process efficiency

2.1 Literature review of moving heat source analytical models

The aim of this review is to identify in the literature of laser material processing an analytical model which can be employed to characterise the heat transfer mechanisms in the SLM process under the action of either CW or PW emission modes in view of the efficiency estimate. An analytical model is used because it is the proper compromise between time/cost of development and accuracy in the estimate of heat transfer. The first analytical solution to a moving point heat source was determined by Carslaw and Jaeger (1959) and studied by Rosenthal (1941, 1946) for the welding technology. In literature, there have been several developments and applications of the moving heat source solutions. The determination of the temperature distribution through the analytical solution of the Rosenthal equation has led to a greater understanding of the solidification phenomena, micro-structure formation and heat transfer mechanisms as well as predictions regarding the shape and size of weld beads, cut kerfs and melt pool formation. Cline and Anthony (1977) were amongst the first to apply Rosenthal type analytical solutions for the laser heat treatment and melting of metallic materials, followed in the next years by Eagar and Tsai (1983) for the prediction of weld pool dimensions and by Ashby and Easterling (1984) for the hardening of steel surfaces.

In the study of the SLM process there have been few applications of analytical thermal models, as reported by Zeng et al. (2012). Amongst these, the moving heat source solution has been used to represent the Selective Laser Sintering process by Singh et al. (2009). The solution considers a Gaussian spatial distribution (derived from Ashby and Easterling (1984)) but does not take into account the possibility of temporal modulation of the heat source. Therefore, in order to compare emission modes a heat transfer model capable of considering a temporal variation of the laser power input should be taken into account.

With reference to the moving heat source problems, the solution for the temperature field generated by a pulsed Gaussian distributed heat source was presented by (JunChang, Langlade, and Vannes 1999) for the study of PW laser heat treatment. A more rigorous approach to the modelling of PW travelling heat sources was undertaken by Dowden (2001). On the other hand, the solution by Vishnu et al. (1991) for the modelling of the heat flow during Gas Tungsten Arc welding, presents both a complete mathematical derivation and experimental evidence confirming the validity of the model. Hence, amongst all the analytical models reviewed, Vishnu et al. (1991) can be considered as the most appropriate to model the interaction of a PW Gaussian distributed laser source with a metallic powder bed.

2.2 Modelling of powder bed thermal and physical properties

Amongst the hypotheses of analytical solutions to moving heat source problems, there is the consideration of a homogeneous, isotropic material with constant thermal and physical properties. In the proposed modelling of PW SLM, this hypothesis will be maintained and the value of specific heat capacity, thermal conductivity and density at a mean temperature between ambient temperature and solidus temperature of AISI 316L will be considered (i.e. at 700 °C, as shown in the values are reported in Table 1), using the values determined by Mills (2002) as a reference.

Table 1. Thermal and physical properties of bulk AISI 316L at 700 °C recorded by (Mills 2002)

Property	Symbol	Units	Value at 700 °C
Bulk solid thermal conductivity	k_s	$Wm^{-1}K^{-1}$	25.1
Specific heat capacity	c_p	$Jkg^{-1}K^{-1}$	600
Bulk solid density	ρ_s	kgm^{-3}	7628
Bulk solid thermal diffusivity	α_s	m^2s^{-1}	5.48×10^{-6}

In order to determine the thermal conductivity of the powder bed (ρ_p), the model by Sih and Barlow (2004) will be employed. This approach has been previously used in the modelling of the laser powder interaction (as for example in the work by Denlinger et al. (2016) or Vail et al. (1996). Amongst the main input parameters to the model by Sih and Barlow (2004) is the relative density, which is fundamental in determining the compactness of the powder bed. In literature, the value of relative density θ with respect to the bulk solid, defined as the ratio between ρ_p and ρ_s, has often been taken as $\theta = 0.5$ and will be assumed also in this study. Matsumoto et al. (2002) used this value for the finite element modelling of single layer deposition of Ni-based superalloys, Antony et al. (2014) for the analytical modelling of single track deposition of stainless steel while Contuzzi et al. (2011) for the development of a finite element model for the SLM of AISI 316L. On the other hand, the specific heat capacity of the powder bed remains unvaried with respect to the bulk solid value. Overall, the values of the thermal and physical properties implemented in the model are reported in Table 2.

Table 2. Thermal and physical properties of powder bed of AISI 316L at 700 °C

Property	Symbol	Units	Value at 700 °C
Powder bed thermal conductivity	k_p	$Wm^{-1}K^{-1}$	0.46
Specific heat capacity	c_p	$Jkg^{-1}K^{-1}$	600
Powder bed density	ρ_p	kgm^{-3}	3814
Powder bed thermal diffusivity	α_p	m^2s^{-1}	2.02×10^{-7}

The final consideration regarding the effective spatial domain of the solution is that the powder bed is not infinite (a different assumption to the model by Vishnu et al. (1991)). Due to the strong discontinuity in material properties between powder bed and bulk substrate it is possible the hypothesis of negligible conductive heat transfer at the bottom boundary was made. Hence, the physical domain is representable in the present model by applying the method of images which consists in the reflection of the mathematical solution between the top and bottom boundary of the domain and the summing up of the reflections to obtain the final solution (as represented graphically in Figure 1).

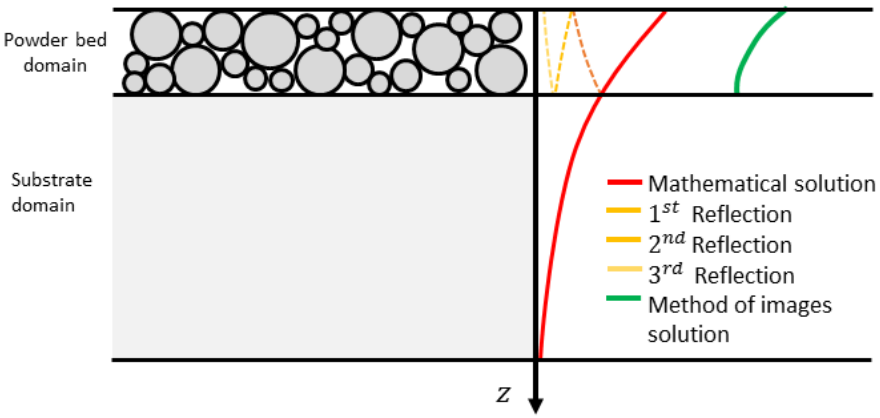

Figure 1. Applying the method of images to represent the powder bed domain

2.3 Analytical modelling of efficiency in SLM

As previously introduced, Vishnu et al. (1991) determined the solution for the temperature field generated by a pulsed wave Gaussian distributed moving heat source and the solution may be employed to represent the pulsed wave selective laser melting process. The heat source considered in the model is moving at constant velocity v (with respect to the absolute coordinate system indicated in Figure 2) and it is temporally modulated as shown in Figure 3.

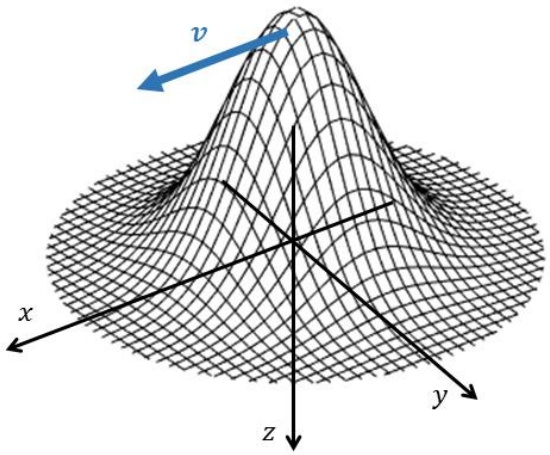

Figure 2. Gaussian distributed heat source moving at constant velocity v in the x-direction with respect to absolute coordinate system (x,y,z)

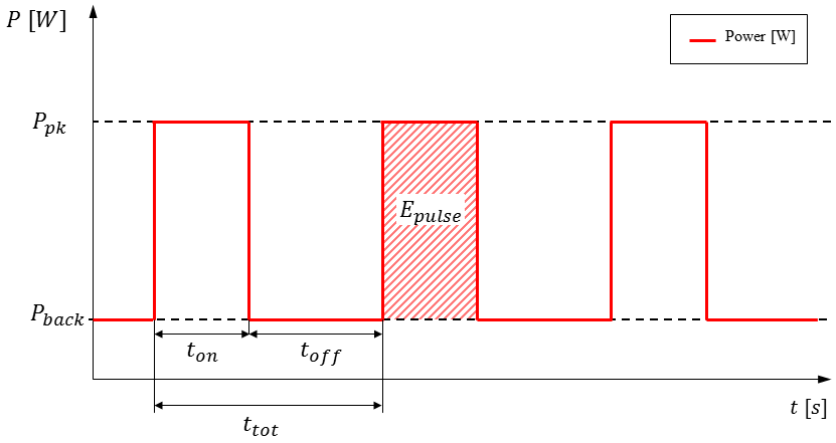

Figure 3. Temporal profile of moving heat source

The mathematical solution (indicated in equation (1)) is given by the contribution of the peak power (P_{pk}) and the background power (P_{back}) of the PW emission (schematised in Figure 3) which respectively causes increases in temperature of ΔT_p and ΔT_b. Since the comparison between pulsed wave emission and continuous wave emission is the focus of the present study, when considering CW emission, the background power will be taken as equal to the peak power (i.e. $P_{back} = P_{pk}$) whereas in the case of PW emission the contribution will be null (i.e. $P_{back} = 0$).

$$T(x, y, z, t) = T_0 + \Delta T_p + \Delta T_b \tag{1}$$

The peak and background power contributions to the temperature distribution of the heat flow model by Vishnu et al. (1991) are reported in equations (2) and (3) whilst the integration limits and integration constants are reported in Appendix A.

$$\Delta T_p = \eta(\delta, v)\frac{4P_{pk}}{\rho_p c_p \left(4\pi\alpha_p\right)^{3/2}} \cdot \exp\left[-\frac{v\xi}{2\alpha_p} - \frac{v^2 t_0}{4\alpha_p}\right] \cdot \sum_{n=1}^{N_p} \int_{a_n}^{b_n} \frac{1}{1+\mu^2} \exp\left[-\frac{M}{\mu^2} - \frac{N}{1+\mu^2} - P\mu^2\right] d\mu \qquad (2)$$

$$\Delta T_b = \eta(\delta, v)\frac{4P_{back}}{\rho_p c_p \left(4\pi\alpha_p\right)^{3/2}} \cdot \exp\left[-\frac{v\xi}{2\alpha_p} - \frac{v^2 t_0}{4\alpha_p}\right] \cdot \sum_{n=1}^{N_p} \int_{a_n}^{b_n} \frac{1}{1+\mu^2} \exp\left[-\frac{M}{\mu^2} - \frac{N}{1+\mu^2} - P\mu^2\right] d\mu \qquad (3)$$

The efficiency coefficient η is multiplicative of the temperature distribution and is representative of the heat transfer mechanisms due to the gaussian distributed source acting upon the powder bed. Therefore, its variation will be representative of the melting efficiency and will be characterised with respect to process parameters, in particular on the scanning speed and duty cycle. In order to demonstrate, the capability of the model of predicting a time-dependent temperature distribution an example is shown in Figure 4. It is possible to view heating and cooling cycles generated by a pulsed heat input on the surface (i.e. z=0) of an AISI316L powder bed (processing parameters for this specific condition: v=162 mm/s, P_{pk}=244 W, δ=0.4, t_{on}=200 μs and hypothesised efficiency coefficient η=0.19).

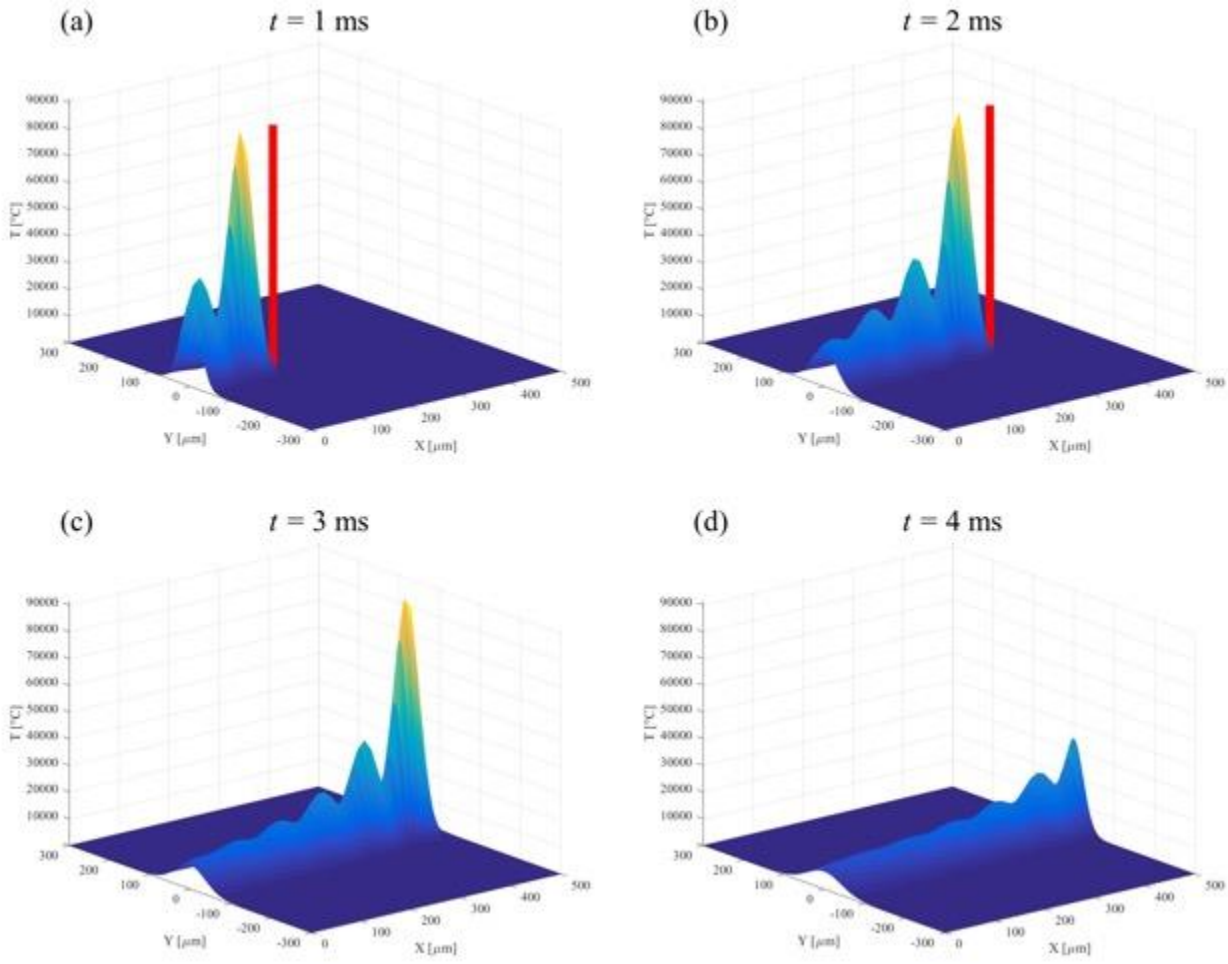

Figure 4. Temperature distribution in spatial simulation domain (*x* and *y* coordinates) at successive time instants *t*: (a) *t*=1 ms (b) *t*=2 ms (c) *t*=3 ms and (d) *t*=4 ms. Position of heat source when on indicated by red line.

2.4 Model implementation and calculation of melting efficiency

In order to determine the variation of the efficiency coefficient with respect to process parameters, the simulated track width (w_{melt}) was estimated from the temperature distribution and then compared with the i-th experimental result (w_i). The corresponding value of efficiency η that yielded the i-th experimental measurement was thus considered for the specific experimental condition. In general, the specific point with coordinates (x_j, y_j, z_j) at a specific time instant t, was considered molten if its temperature was greater than the solidus temperature of the material (i.e. $T(x_j, y_j, z_j, t) > T_{solidus}$). The model was solved on the XY plane with coordinate Z=0 μm (i.e. where the heat source is applied), taking into account a single reflection of the mathematical solution (considering a layer thickness of

50 µm) since the contribution of higher order reflections was negligible (as resulted from preliminary calculations). The simulation domain in the X-axis was of 3 mm whereas a positive and negative variation of 300 µm was employed for the Y-axis domain. The spatial simulation domain used for the analytical model is reported in Table 3.

Table 3. The spatial domain implemented in the analytical model

	X-axis	**Y-axis**	**Z-axis**
Domain	{0:3000} µm	{-300:300} µm	{0,100} µm
Resolution	100 µm	1 µm	100 µm

The solution to the analytical model by Vishnu et al. (1991) is time dependent therefore, also the simulated track width will vary with time. Accordingly, in order to view the expansion and contraction of the simulated melt pool area correctly, the time domain considered was of at least 40 ms after the laser beam completed the single track (with a temporal resolution of 2 ms). Hence, the simulated track width w_{melt} was considered as the highest expansion in the y-direction reached by the melt area within that time domain.

Since the temperature distribution is dependent on its multiplicative efficiency coefficient η, also the simulated track width will be dependent on η (i.e. $w_{melt} = w_{melt}(\eta)$). Hence, from the experimental data replicates (with process parameters corresponding to the simulated condition) it is possible to determine corresponding values of the efficiency coefficient and determine the statistical variation of η which will be representative of the process variability. This operation can be viewed graphically in Figure 5. By repeating this procedure for each experimental condition, it is then possible to determine the variation of η with respect to process parameters.

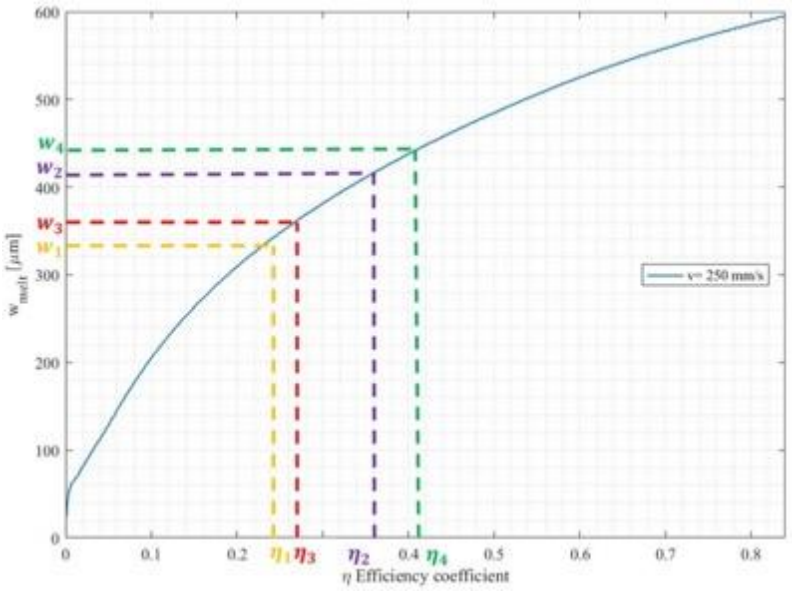

Figure 5. Graphical representation of method employed to determine η_i from *i-th* experimental replicate w_i for a given experimental condition. Simulated track width as a function of η ($w_{melt} = w_{melt}(\eta)$) in blue. Experimental measurements w_1, w_2, w_3, w_4 respectively in yellow, purple, red and green.

2.5 Model for constant energetic input comparison

The definition of equivalent process conditions for modulated and continuous emission regimes in the SLM process is formulated from the consideration that a given energetic input is required to melt a specific volume of material. A model to equate the energy delivered by the laser source during the scanning of a single track respectively with CW and PW emission was developed by the authors of the present work and presented in a previous publication (Caprio et al. (2018)). Modulated emission with contemporary fiber lasers often consists in operating the laser source at the same peak output power of CW emission whilst employing a fast-switching of the pumping diodes to turn on and off the laser emission. The main regulating parameters are the duration of a single laser pulse (t_{on}) and the duty cycle (δ) defined as:

$$\delta = \frac{t_{on}}{t_{on} + t_{off}} \tag{4}$$

Where t_{off} is the time period that the laser is not emitting between two successive pulses (as analogously shown in Figure 3 for the modelling of the temporal profile of the heat source). If CW emission is taken as the reference operating condition, the effect of modulating the laser emission

(i.e. using a value of duty cycle lower than 1, which corresponds to CW emission) will be of delivering a lower average power to the powder bed. Therefore, in order to deliver the same energy density, the laser scanning velocity must be regulated accordingly as defined by the model previously developed:

$$v_{pw} = \frac{P_{avg}}{P_{cw}} \cdot v_{cw} \quad (5)$$

As already mentioned, the process parameters which allow the compare the single track deposition with different emission modes are the scanning speed *v* and average power output *P* of the laser beam. The pedices *pw* and *cw* in the equation indicate the emission mode. P_{cw} will correspond to the instantaneous power output of the laser source during continuous wave emission, whereas P_{avg} indicates the average power delivered with modulated emission.

In the present work, in order to simplify the comparison of the different emission modes, the scan speed of CW emission is taken as reference for a given energetic input, v_{cwEQ} (the value of scan speed was regulated accordingly for the PW emission conditions).

3. Materials & methods

3.1 Material

AISI 316L stainless steel was used as feedstock material under the form of gas atomised powder with mean particle size 32 μm and nominal material density 8.1 g/cm3 (Cogne Acciai, Brescia, Italy).

3.2 Selective laser melting system

The SLM system used to deposit the single tracks was an house developed machine, namely project *Powderful*, whose working mechanism have been presented in previous publications by Demir et al. (2017). The prototype system was equipped with a single mode fibre laser source (IPG Photonics YLR-150/750-QCW-AC, Cambridge, MA, USA). The emission wavelength corresponded to λ=1070 nm and a P_{pk}=244 W maximum peak power output (measured after the optical chain). The light beam deflection onto the powder bed was obtained through the use of a scanner head (El.En. Scan Fiber,

Florence, Italy) whilst the beam trajectories were designed using LogoTag software (Taglio, Piobesi d'Alba, Italy). The emission light was collimated using a 60 mm lens and focused onto the build plate with a 255 mm f-theta lens. Theoretical calculations allowed to estimate the beam waist diameter on the focal plane (d_0) as 55 µm.

Table 4. Principal specifications of the in-house developed SLM system, project *Powderful*

Maximum peak power, P_{pk}	244 W
Laser emission wavelength, λ	1070 nm
Beam quality factor, M^2	1.1
Beam waist diameter, d_0	55 µm
Build substrate dimension (LxWxH)	60x60x20 mm^3

The characteristics of the flexible prototypal system are summarized in Table 4. LabVIEW software (National Instruments, Austin, TX, USA) was used to control the automated powder bed deposition of project *Powderful*. Laser processing was conducted in inert atmospheric conditions that were obtained by three successive purging procedures of the closed chamber (consisting in applying a vacuum down to 50 mbar then introducing high purity Ar).

3.3 Experimental plan

The experimental campaign to evaluate the effect of pulsed and continuous emission was planned at fixed energetic deposition levels. The powder bed layer height was kept at 50 µm (a value typical of SLM processing of AISI 316L), the focal point was positioned at the surface of the powder bed and peak power of laser emission was fixed at the laser source's maximum level of diode pumping current (corresponding to a peak power emission P_{pk}=244 W). During preliminary experimentation, stability conditions at single layer deposition with continuous wave emission were established at scan velocities of 50 and 450 mm/s (identified in the previous publication by Caprio et al. (2017)). Consequently, three levels of equivalent scan speed were chosen (respectively fixed at 50, 250 and

450 mm/s). With modulated emission, two levels of duty cycle (δ=0.4 – 0.6) and two levels of pulse duration (t_{on}=100 – 200 µs) were varied. Effective values of scanning speed are listed in Table 5 (t_{on} does not affect P_{avg} therefore does not determine a change in the effective scan speed). As can be extrapolated from Table 5, the lower average power emitted during modulated emission implies that the laser source must travel more slowly in order to deliver the same energetic input in comparison to CW emission. Fixed and varied factors in the experimentation plan are reported in Table 6. Variation in terms of number of deposited layers (N_{layers}=1;5;10) was also tested and four replicates of each experimental condition were run.

Table 5. Effective values of scan speed respectively for modulated and CW emission

v_{cw} [mm/s]	v_{pw} at δ=0.6 [mm/s]	v_{pw} at δ=0.4 [mm/s]
50	28	18
250	142	90
450	256	162

Table 6. Constant and variable factors of the experimental plan

Constant factors	**Value**
Single track length, l [mm]	30
Layer height, l_t [µm]	50
Peak power, P_{pk} [W]	244
Focal position, Δz [mm]	0
Varied parameters CW emission	**Value**
Scan speed, v_{cw} [mm/s]	50; 250; 450
Varied parameters PW emission	**Value**
Scan speed, v_{cwEQ} [mm/s]	50; 250; 450
Duty cycle, δ	0.4; 0.6
Pulse duration, t_{on} [µs]	100; 200

3.4 Single track characterisation

Track morphology was acquired using focus variation microscopy (Infinite Focus from Alicona, Graz, Austria) which allowed for track width (w) and volume measurements (V). The measurements were conducted onto the whole of the substrate plate employing a 5X magnification. The vertical and lateral resolutions were respectively estimated as 0.5 µm and 7 µm. A representative digital reconstruction of the single tracks is shown in Figure 6 (a) along with the track width measurement procedure (Figure 6 (b-c)). The track width measurements were used successively to calculate the efficiency with the analytical model. From the volume measurements, it was also possible to calculate the single track build rate of the process BR, defined as:

$$BR = \frac{V \cdot v}{N_{layers} \cdot l} \tag{6}$$

where v is the scan speed, N_{layers} the number of layers of deposited material.

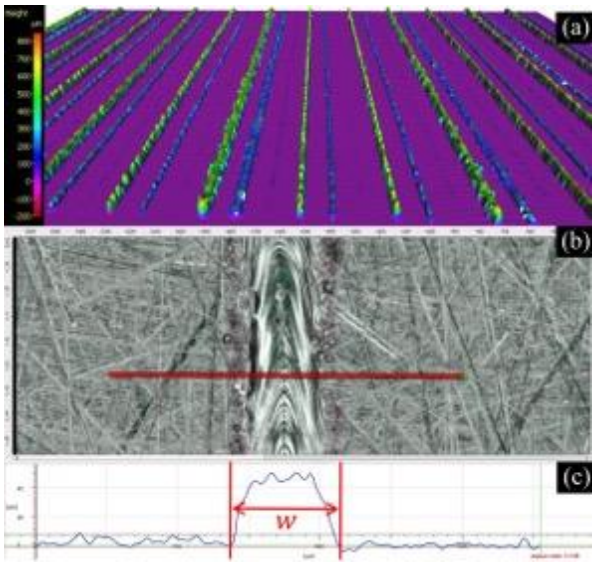

Figure 6. (a) Digital reconstruction of single tracks plate obtained using focus variation microscopy (b) top view of one single track; red line indicates data selection for width measurement (c) single track profile obtained from previous data selection for width measurement

The deposited single tracks were cut transversally to provide metallographic cross-sections which were prepared by polishing and chemical etching with a tripartite solution of hydrochloric acid, nitric

acid and distilled water. The cross sections were photographed using optical microscopy with a 2.5X objective (Ergolux 200 from Leitz, Wetzlar, Germany).

4. Experimental campaign results

4.1 Volume of deposited material and build rate

The variation of track volume with respect to equivalent scanning speed, duty cycle and pulse duration is reported in Figure 7. The data shows an analogous densification behaviour with increasing number of layers of deposited material. The effect of pulse duration on the deposited volume was negligible with respect to duty cycle and v_{cwEQ} therefore, for the sake of clearness, is not reported graphically.

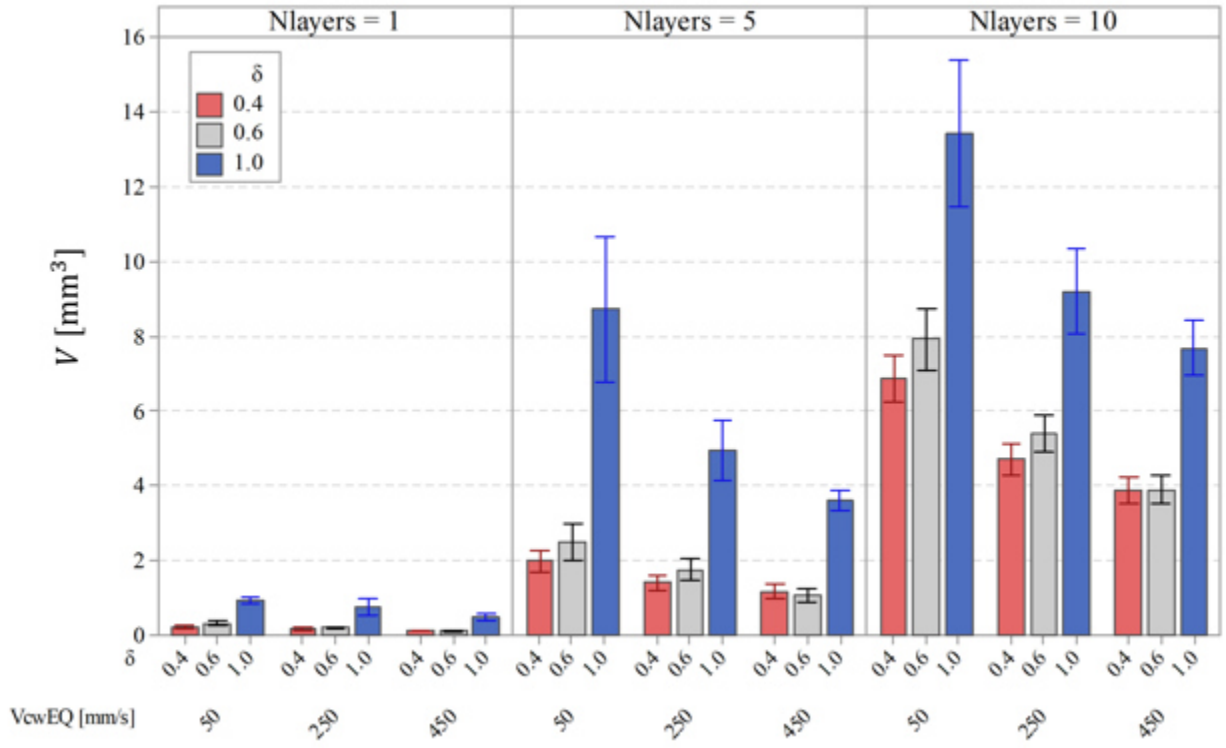

Figure 7. Track volume as a function of process parameters and number of layers of deposited material. Error bars are one standard error from the mean. Red and grey colour indicates pulsed wave emission respectively with duty cycle levels of 0.4 and 0.6, blue colour indicates continuous wave emission corresponding to δ=1.

Experimental measurements show that with increasing values of energy density (i.e. lower values of equivalent scanning speed) a greater volumetric deposition can be witnessed. As can be clearly denoted in Figure 7, analogous behaviour can be observed in the duty cycle effect where the highest

deposition is obtainable with CW emission (i.e. δ=1). On the other hand, modulated emission has a positive effect in reducing process variability, indicating that this processing condition is more appropriate when greater control is required.

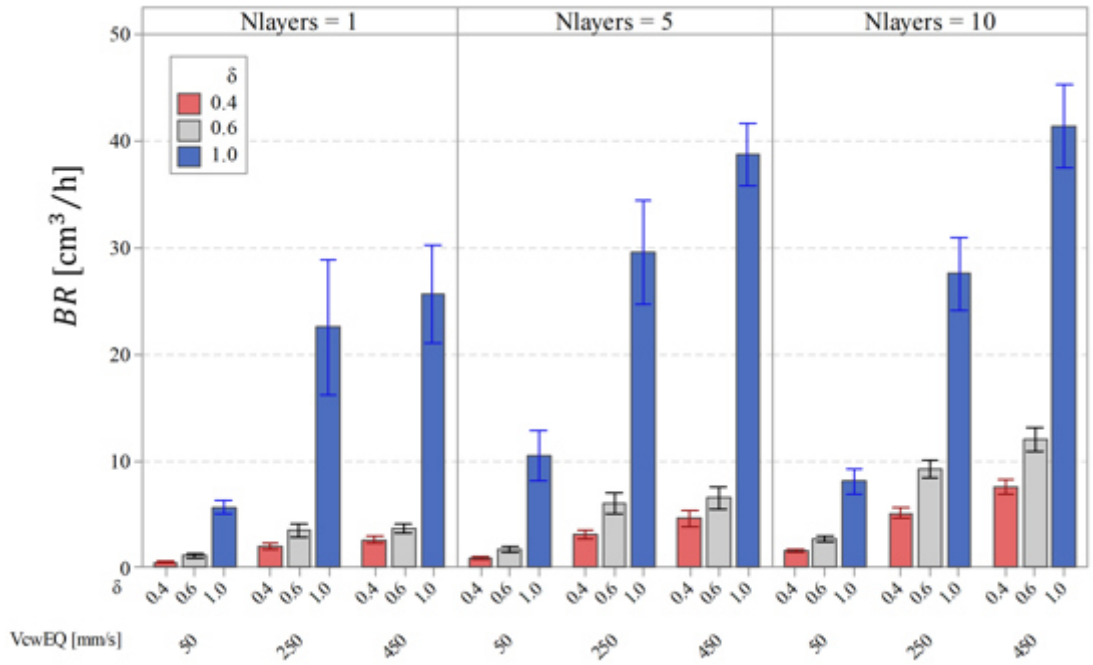

Figure 8. Build rate as a function of process parameters. Error bars are one standard error from the mean. Red and grey colour indicates pulsed wave emission respectively with duty cycle levels of 0.4 and 0.6, blue colour indicates continuous wave emission corresponding to δ=1.

The effective values of scan speed are lower in the case of PW emission, since to deliver a constant energetic input the laser beam must advance more slowly (as previously indicated in Table 5). The combined effect of this aspect and the changes in deposited volume related to different emission mode causes the build rate to be significantly affected. Thus temporal modulation yields notably lower values of build rate whereas CW emission resulted the most productive (as reported graphically in Figure 8). The build rates reported in the present research are comparable in terms of magnitude to values reported in literature for the realisation of bulk AISI 316L specimen although differences can be accounted for due hatching distance parameter (Wang et al. 2017).

4.2 Track width and cross section analysis

In Figure 9, the variations of the width of single tracks with respect to process parameters is shown. Analogously to the volume, it was possible to denote that pulse duration was not significant in affecting the measured variable therefore its variation was not reported graphically. Furthermore, the results depict a clear increase in terms of deposition width at increasing values of duty cycles. The track width is a fundamental parameter in defining the resolution of the SLM process and its capability of realising fine features, as indicated by Yadroitsev et al. (2010, 2007). As a matter of fact, the use of temporal modulation coincides with a lower process variability with respect CW emission which suggests that this might be the appropriate strategy for the realisation of detailed features.

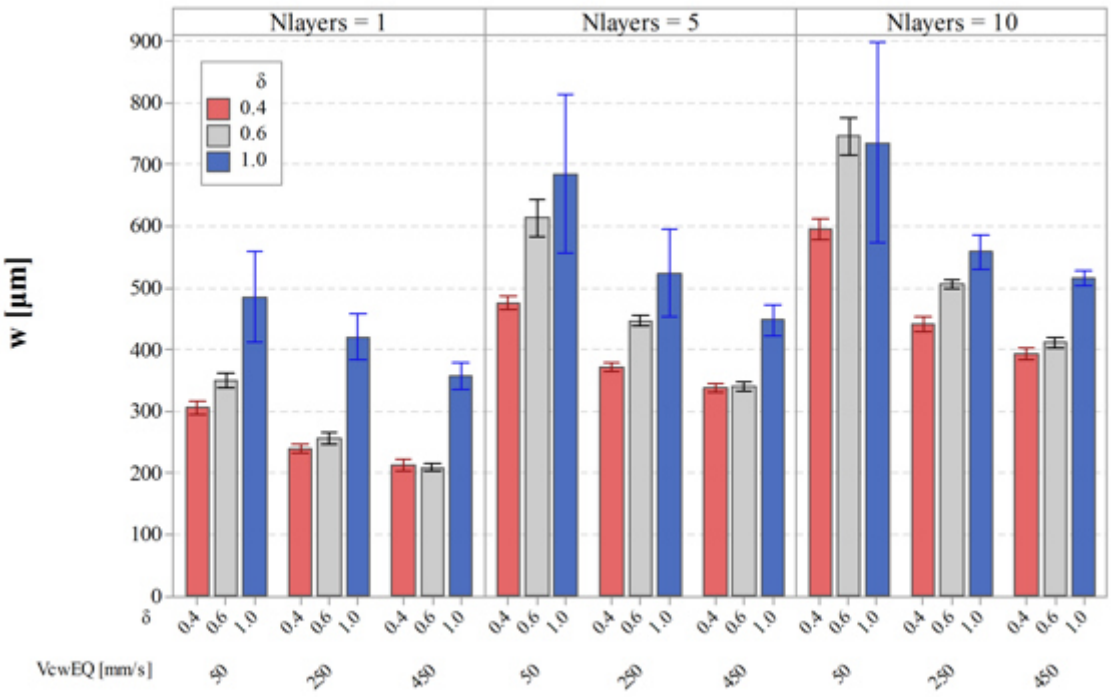

Figure 9. Width of single tracks as a function of process parameters and number of deposited layers. Error bars are one standard error from the mean. Red and grey colour indicates pulsed wave emission respectively with duty cycle levels of 0.4 and 0.6. Blue colour indicates continuous wave emission corresponding to δ=1.

In accordance with previous single track studies by Yadrotisev et al. (2013, 2015), track width decreases with higher values of scanning speed. This phenomenon was reported both with continuous wave and pulsed wave emission. By observing the cross sections of the deposited single tracks

(representative conditions are shown in Figure 10 for single layer deposition and in Figure 11 for 10 layers), it is possible to extract information regarding track morphology in terms of width and depth of the dilution zone.

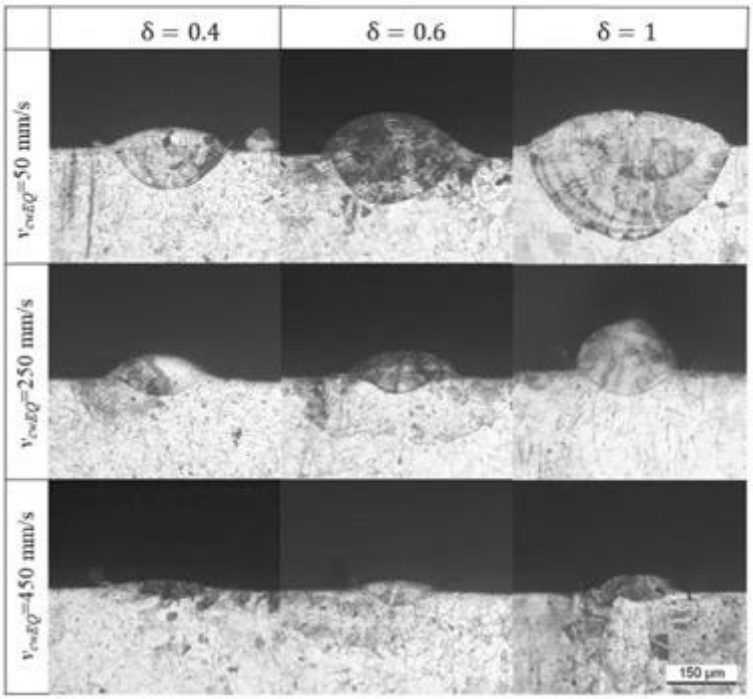

Figure 10. Metallographic cross-sections of 1-layer single track depositions at varying levels of v_{cwEQ} and emission modes.

It is arguable that the trends recorded for the volumetric deposition and track width measured using focus variation microscopy can be denoted in the cross-section observations: the depth of the dilution area is notably more restricted at elevated values of equivalent scanning speed and lower values of duty cycle. Furthermore, dilution zone width increases with greater energetic input, once again in agreement with observations from Yadroitsev et al. (2013).

The first signs in terms of process instability can be denoted from the cross-sections at v_{cwEQ}=450 mm/s, shown in Figure 11. These defect can possibly be generated by insufficient energetic input which determines an unstable melt pool formation due to higher surface tension forces which can give rise to the balling phenomenon as was also determined experimentally by Li et al. (2012). This

hence also brings supporting evidence to the reasons for porosity formation due to melt flow instabilities as discussed by Qiu et al. (2015).

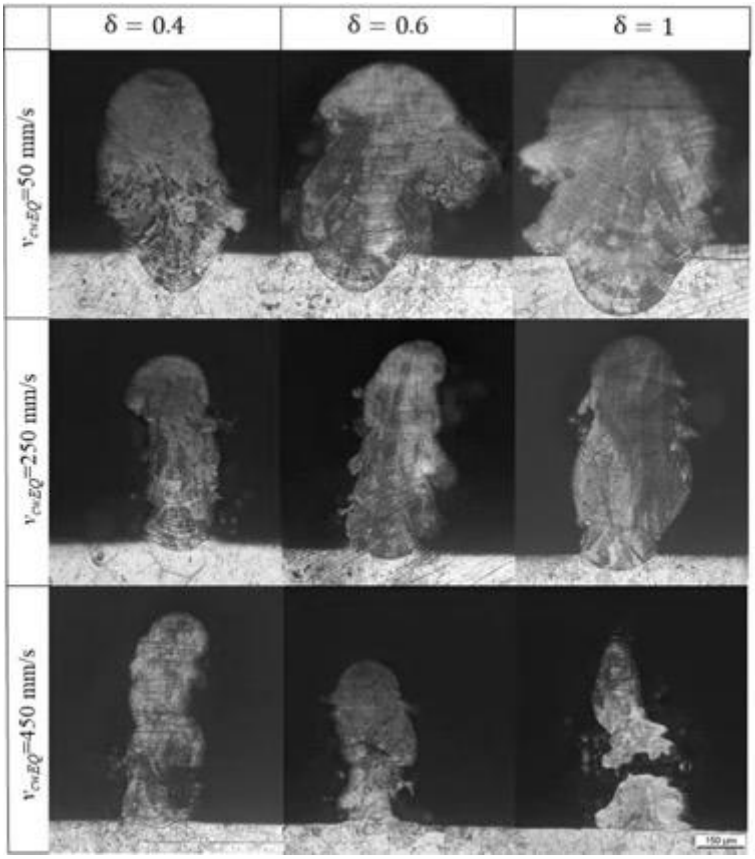

Figure 11. Metallographic cross-sections of 10-layer single track depositions at varying levels of v_{cwEQ} and emission modes.

4.3 Melting efficiency

The analytical model yields as a result the trend of the process melting efficiency at different levels of emission modes and equivalent scanning speed. The simulations indicate a significant increase in η at higher levels of duty cycle and increasing values of equivalent scanning speed (i.e. lower energetic deposition levels). In order to characterise the trend of the process efficiency at different energetic values and under varying temporal emission modes, a regression model was determined (reported in equation 16 whilst the full statistical analysis is reported in Table 7):

$$ln(\eta) = -3.8094 + 0.008691\, V_{cwEQ} - 10^{-5} V_{cwEQ}^2 + 1.0178\, \delta^2 \quad (7)$$

Table 7. Regression analysis for process efficiency coefficient

Source	DF	Seq SS	Adj SS	Adj MS	F-Value	P-value
Regression	3	28.1829	28.1829	9.39429	265.60	0.000
v_{cwEQ}	1	19.9696	6.1187	6.11871	172.99	0.000
v_{cwEQ2}	1	2.2701	2.2701	2.2701	64.18	0.000
δ_2	1	5.9432	5.9432	5.9432	168.03	0.000
Error	56	1.9807	1.9807	0.03537		
Lack-of-Fit	5	0.3709	0.3709	0.07418	2.35	0.054
Pure Error	51	1.6098	1.6098	0.03156		
Total	59	30.1636				

R_2=93.4%, R_{2adj}=93.1%, R_{2pred}=92.4%

In order to depict graphically the response surface generated by the regression equation and relative confidence intervals, the following equation was employed as defined by Montgomery (2017):

$$y(\mathrm{x}_0) - t_{\frac{\alpha}{2},n-p}\sqrt{\hat{\sigma}^2\mathrm{x}_0'(\mathrm{X}'\mathrm{X})^{-1}\mathrm{x}_0} \leq \mu_{y|x_0} \leq y(\mathrm{x}_0) + t_{\frac{\alpha}{2},n-p}\sqrt{\hat{\sigma}^2\mathrm{x}_0'(\mathrm{X}'\mathrm{X})^{-1}\mathrm{x}_0} \quad (8)$$

Where y is the regression equation, n is the number of observations, p the number of regression coefficients, t the t-student distribution inverse function, α the confidence level, $\hat{\sigma}$ the estimated standard deviation, X the design matrix with the levels of the independent variables of the experiment, x_0 the vector of the condition at which the regression equation is being calculated.

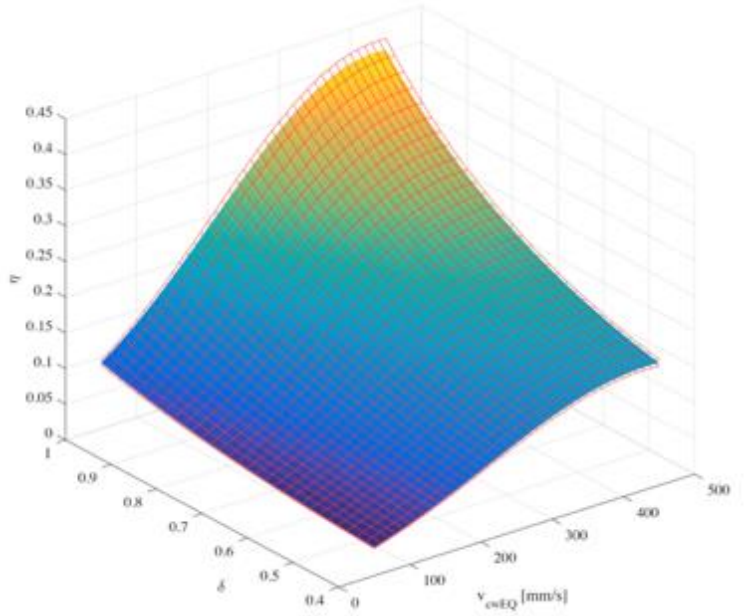

Figure 12. Response surface of the regression equation. Red planes indicate minimum and maximum confidence intervals of the response surface

The response surface is shown in Figure 12. The model fits the data well as expressed by the high R_{2adj} value and the narrow confidence intervals shown in the response surface. Both of the examined parameters have a second order relationship with process efficiency. The sign of the second order regressor coefficients indicates how the parameters interact with the process efficiency. The increase in duty cycle provides a rapid increase in the process melting efficiency reaching its effective peak at CW emission. On the other hand, the increase in scan speed is expected to provide the maximum efficiency at a certain point and then drop as indicated by the negative value of its second order coefficient. Such condition is coherent with the physical reality, since the process will eventually yield lack of fusion due to the lower energetic input.

5. Discussion

The volume and track width variations underline a significantly high difference in the powder bed solidification when exposed to temporally modulated laser beams. Process melting efficiency can be linked to different components regarding the optical and thermal efficiencies, as well as mechanical instabilities generated due to the emission region being used.

Firstly, an improved optical coupling between laser emission and melt pool during continuous wave emission as was suggested for the analogous process of laser welding by Assuncao and Williams (2013). It can be expected that the fraction molten pool remains stably at a higher temperature, which can improve the optical absorption, as stated by Steen and Mazumder (2010). On the other hand, this might be lower during pulsed wave emission due to the formation of stronger recoil pressures which are reported by Mumtaz and Hopkinson (2010) during PW SLM. Effectively, this reduced interaction can be symptomatic of the more contained dilution zone observable in the cross-section of single tracks obtained with modulated emission (shown in Figure 10). As Qiu et al. (2015) state, Marangoni forces and recoil pressure can be detrimental for the solidification phenomena, thus explaining the lower volume of material deposited with PW emission. Analogous conclusions regarding defect

formation and lower densification were achieved by the authors (Demir et al. (2017)) in a previous work which employed PW emission, supporting the observations made in the present research. In general, it might be stated that continuous wave emission is characterised by more efficient heat transfer mechanisms that can be beneficial for higher material deposition rates. Yet this emission condition also coincides with a higher process variability terms of track width and volumetric deposition as can be seen from the greater spread of the results for CW emission respectively reported in Figure 7 and Figure 9 which might be detrimental for the final roughness of SLM produced specimen.

On the other hand, the analytical model shows that heat transfer efficiency increases at higher values of equivalent scanning speed (i.e. lower energetic conditions). Such increase can be attributed to a more efficient use of the released energy over a limited thickness, reducing the remelted layer region. Another important factor is the optical absorptivity that may vary due to the scan speed. A maximum absorption is achieved at Brewster angle, where for molten iron and the wavelength of a fiber laser is approximately 80°. Lower scan speeds correspond to an increase in the glancing angle resulting in a sudden drop of absorptivity as Mahrle and Beyer (2009) state. A similar effect can be observed if the molten pool oscillates due the repetitive heating and cooling cycles induced by the PW regime. On the other hand, interplay between increased optical efficiency and reduced melting capability exists. Further increases in scanning speed can also generate melt pool instability due to the balling phenomena caused by the higher surface tension and Marangoni forces, as observed experimentally by Li et al. (2012) and Yadroitsev et al. (2007) in the SLM processing of stainless steels. Accordingly, also Qiu et al. (2015) support this view. As Khairallah and Anderson (2014) predict through their model that lower values of scan speed allow the achievement of full melting of the powder bed avoiding residual porosity. However, increasing the energetic input by lowering the scan speed aspect is detrimental with regards to the obtainment of fine features. On the other hand, higher scan speeds

might generate inter-layer porosity formation due to a lower remelting of the previous layer, as observable in the cross-sections of the deposited single tracks of Figure 10 and in Xia et al. (2017). High speed imaging observations of the selective laser melting process under analogous conditions, were conducted by the authors of the present research Caprio et al. (2018). Results indicated that melt pool dimension are effectively more confined using pulsed wave emission although this is coincides with an intermittent behaviour of the melt area due to the pulsating nature of the power input. On the other hand it was possible to denote the higher stability of the melt pool achievable with CW emission which however yielded a perturbation of the powder bed causing a denudation phenomena. The higher process variability in terms of track width and volumetric deposition recorded in the present work can thus be found to coincide with the greater perturbation recorded through high speed observations of the previous research. Moreover, the process efficiency determined with the analytical model is descriptive of higher stability and thus a more efficient heat transfer mechanisms occurring during the single track deposition.

Further considerations should be made when taking into account the effect of multi-track scanning since there is a thermal build up phenomena caused by the heat affected zone of previous scan tracks as evidenced by Criales et al. (2017). The partial overlap between the adjacent track also varies the material properties under the scanning laser beam, since both solid and powder material is processed. Indeed, the scan strategy as well as the geometry can have a significant impact on the process efficiency, which can be combined with the effect of the emission regime.

6. Conclusions

In this work, the process efficiency of CW and PW emission modes in single track selective laser melting of AISI 316 powder was studied experimentally and by means of an analytical model. The experimental work clearly indicates the improved melting capacity by CW emission, while the

analytical model provides a clear indication to the process efficiency. The principal outcomes of this work can be listed as:

- Volumetric deposition with CW emission was from two to three times higher than with modulated laser input.
- Build rate was also significantly higher in the case of CW emission (up to 40 cm^3/h), also due to the reduced effective scanning speed that must employed for a fixed energetic deposition during PW emission.
- Process resolution, determined through track width measurements was notably increased with power modulated emission (from 350 µm to 200 µm at single layer and low energetic deposition condition).
- Process efficiency estimated through the analytical model resulted three times higher with CW emission and yielded greater values at higher levels of scan speed ($\eta \approx 0.35$). Optical coupling between melt pool and laser radiation is considered the main influential parameter. Increased scan speed improves the efficiency intrinsically by limiting the remelted region as well as a possible improvement in the optical absorption. At higher scan speeds a limit exists due to the melt pool stability due to the insurgence of the balling phenomenon.

As the SLM technology progresses in the industrial world, the need for more flexible systems able to process both bulk and fine geometries will be essential. The combination of the two emission regimes is applicable to the vast majority of the implemented laser sources, while the part programming and trajectory planning require further attention.

7. Acknowledgments

The authors gratefully acknowledge IPG Photonics Italy, El.En, and Taglio for the technical support. This work was supported by European Union, Repubblica Italiana, Regione Lombardia and FESR for the project MADE4LO under the call "POR FESR 2014-2020 ASSE I - AZIONE I.1.B.1.3".

8. References

Aboulkhair, Nesma T., Ian Maskery, Chris Tuck, Ian Ashcroft, and Nicola M. Everitt. 2016. "On the Formation of AlSi10Mg Single Tracks and Layers in Selective Laser Melting: Microstructure and Nano-Mechanical Properties." *Journal of Materials Processing Technology* 230:88–98.

Antony, Kurian, N. Arivazhagan, and K. Senthilkumaran. 2014. "Numerical and Experimental Investigations on Laser Melting of Stainless Steel 316L Metal Powders." *Journal of Manufacturing Processes* 16(3):345–55. Retrieved (http://dx.doi.org/10.1016/j.jmapro.2014.04.001).

Ashby, M. F. and K. E. Easterling. 1984. "The Transformation Hardening of Steel Surfaces by Laser Beams-I. Hypo-Eutectoid Steels." *Acta Metallurgica* 32(11).

Assuncao, Eurico and Stewart Williams. 2013. "Comparison of Continuous Wave and Pulsed Wave Laser Welding Effects." *Optics and Lasers in Engineering* 51(6):674–80. Retrieved (http://dx.doi.org/10.1016/j.optlaseng.2013.01.007).

Averyanova, M., E. Cicala, Ph. Bertrand, and Dominique Grevey. 2012. "Experimental Design Approach to Optimize Selective Laser Melting of Martensitic 17-4 PH Powder: Part I – Single Laser Tracks and First Layer." *Rapid Prototyping Journal* 18(1):28–37. Retrieved (http://www.emeraldinsight.com/doi/10.1108/13552541211193476).

Bidare, P., I. Bitharas, R. M. Ward, M. M. Attallah, and A. J. Moore. 2018. "Fluid and Particle Dynamics in Laser Powder Bed Fusion." *Acta Materialia* 142:107–20. Retrieved (https://doi.org/10.1016/j.actamat.2017.09.051).

Bidare, P., R. R. J. Maier, R. J. Beck, J. D. Shephard, and A. J. Moore. 2017. "An Open-Architecture Metal Powder Bed Fusion System for in-Situ Process Measurements." *Additive Manufacturing* 16(June):177–85. Retrieved (http://dx.doi.org/10.1016/j.addma.2017.06.007).

Biffi, C. A., J. Fiocchi, P. Bassani, and A. Tuissi. 2018. "Continuous Wave vs Pulsed Wave Laser Emission in Selective Laser Melting of AlSi10Mg Parts with Industrial Optimized Process Parameters: Microstructure and Mechanical Behaviour." *Additive Manufacturing*. Retrieved (https://doi.org/10.1016/j.addma.2018.10.021).

Binda, B., E. Capello, and B. Previtali. 2004. "A Semi-Empirical Model of the Temperature Field in the AISI 304 Laser Welding." *Journal of Materials Processing Technology* 155–156(1–3):1235–41.

Caprio, Leonardo, Ali Gökhan Demir, and Barbara Previtali. 2017. "Effect of Pulsed and Continuous Wave Emission on the Densification Behaviour in Selective Laser Melting." *39th International Matador Conference* 1–7.

Caprio, Leonardo, Ali Gökhan Demir, and Barbara Previtali. 2018. "Comparative Study between CW and PW Emissions in Selective Laser Melting." *Journal of Laser Applications* 30(3):32305.

Carslaw, Horatio Scott and John Conrad Jaeger. 1959. *Conduction of Heat in Solids*. Clarendon Press.

Ciurana, Joaquim, Luis Hernandez, and Jordi Delgado. 2013. "Energy Density Analysis on Single Tracks Formed by Selective Laser Melting with CoCrMo Powder Material." *International Journal of Advanced Manufacturing Technology* 68(5–8):1103–10.

Cline, H. E. and T. R. Anthony. 1977. "Heat Treating and Melting Material with a Scanning Laser or Electron Beam." *Journal of Applied Physics* 48(9):3895–3900.

Contuzzi, N., S. L. Campanelli, and A. D. Ludovico. 2011. "3D Finite Element Analysis in the Selective Laser Melting Process." *International Journal of Simulation Modelling* 10(3):113–21.

Criales, Luis E. et al. 2017. "Laser Powder Bed Fusion of Nickel Alloy 625: Experimental Investigations of Effects of Process Parameters on Melt Pool Size and Shape with Spatter

Analysis.” *International Journal of Machine Tools and Manufacture* 121(March):22–36.

Demir, Ali Gökhan, Paolo Colombo, and Barbara Previtali. 2017. “From Pulsed to Continuous Wave Emission in SLM with Contemporary Fiber Laser Sources: Effect of Temporal and Spatial Pulse Overlap in Part Quality.” *International Journal of Advanced Manufacturing Technology* 91(5–8):2701–14. Retrieved (http://dx.doi.org/10.1007/s00170-016-9948-7).

Demir, Ali Gökhan, Lorenzo Monguzzi, and Barbara Previtali. 2017. “Selective Laser Melting of Pure Zn with High Density for Biodegradable Implant Manufacturing.” *Additive Manufacturing* 15:20–28. Retrieved (http://dx.doi.org/10.1016/j.addma.2017.03.004).

Demir, Ali Gökhan and Barbara Previtali. 2017. “Additive Manufacturing of Cardiovascular CoCr Stents by Selective Laser Melting.” *Materials and Design* 119:338–50. Retrieved (http://dx.doi.org/10.1016/j.matdes.2017.01.091).

Denlinger, Erik R., Vijay Jagdale, G. V. Srinivasan, Tahany El-Wardany, and Pan Michaleris. 2016. “Thermal Modeling of Inconel 718 Processed with Powder Bed Fusion and Experimental Validation Using in Situ Measurements.” *Additive Manufacturing* 11:7–15. Retrieved (http://dx.doi.org/10.1016/j.addma.2016.03.003).

Dowden, John Michael. 2001. *The Mathematics of Thermal Modeling: An Introduction to the Theory of Laser Material Processing*. CRC Press.

Ducharme, Robert et al. 1994. “The Laser Welding of Thin Metal Sheets: An Integrated Keyhole and Weld Pool Model with Supporting Experiments.” *Engineering and Technology* 27:1619–27.

Eagar, T. W. and N. S. Tsai. 1983. “Temperature Fields Produced by Traveling Distributed Heat Sources.” *Welding Journal* 62(12):346–55.

Gellert, B. and W. Egli. 1988. “Melting of Copper by an Intense and Pulsed Heat Source.” *Journal*

of Physics D: Applied Physics 21:1721–26.

JunChang, Li, C. Langlade, and A. B. Vannes. 1999. "Evaluation of the Thermal Field Developed during Pulsed Laser Treatments: Semi Analytical Calculation." *Surface and Coatings Technology* 115(1):87–93.

Khairallah, Saad A. and Andy Anderson. 2014. "Mesoscopic Simulation Model of Selective Laser Melting of Stainless Steel Powder." *Journal of Materials Processing Technology* 214(11):2627–36. Retrieved (http://dx.doi.org/10.1016/j.jmatprotec.2014.06.001).

Kuo, Tsung-Yuan and Yong-Ding Lin. 2007. "Effects of Different Shielding Gases and Power Waveforms on Penetration Characteristics and Porosity Formation in Laser Welding of Inconel 690 Alloy." *Materials Transactions* 48(2):219–26. Retrieved (https://www.jstage.jst.go.jp/article/matertrans/48/2/48_MRA2006154/_article).

Li, Ruidi, Jinhui Liu, Yusheng Shi, Li Wang, and Wei Jiang. 2012. "Balling Behavior of Stainless Steel and Nickel Powder during Selective Laser Melting Process." *International Journal of Advanced Manufacturing Technology* 59(9–12):1025–35.

Mahrle, A. and E. Beyer. 2009. "Theoretical Aspects of Fibre Laser Cutting." *Journal of Physics D: Applied Physics* 42(17).

Matsumoto, M., M. Shiomi, K. Osakada, and F. Abe. 2002. "Finite Element Analysis of Single Layer Forming on Metallic Powder Bed in Rapid Prototyping by Selective Laser Processing." *International Journal of Machine Tools and Manufacture* 42(1):61–67.

Mills, Kenneth C. 2002. *Recommended Values of Thermophysical Properties for Selected Commercial Alloys*. Woodhead Publishing.

Montgomery, Douglas C. 2017. *Design and Analysis of Experiments*. John Wiley & Sons.

Mumtaz, K. A. and N. Hopkinson. 2010. “Selective Laser Melting of Thin Wall Parts Using Pulse Shaping.” *Journal of Materials Processing Technology* 210(2):279–87.

Mumtaz, Kamran and Neil Hopkinson. 2009. “Top Surface and Side Roughness of Inconel 625 Parts Processed Using Selective Laser Melting.” *Rapid Prototyping Journal* 15(2):96–103. Retrieved (http://www.emeraldinsight.com/doi/10.1108/13552540910943397).

Panwisawas, C. et al. 2015. “On the Role of Thermal Fluid Dynamics into the Evolution of Porosity during Selective Laser Melting.” *Scripta Materialia* 105:14–17. Retrieved (http://dx.doi.org/10.1016/j.scriptamat.2015.04.016).

Qiu, Chunlei et al. 2015. “On the Role of Melt Flow into the Surface Structure and Porosity Development during Selective Laser Melting.” *Acta Materialia* 96:72–79. Retrieved (http://dx.doi.org/10.1016/j.actamat.2015.06.004).

Roehling, Tien T. et al. 2017. “Modulating Laser Intensity Profile Ellipticity for Microstructural Control during Metal Additive Manufacturing.” *Acta Materialia* 128:197–206. Retrieved (http://dx.doi.org/10.1016/j.actamat.2017.02.025).

Rosenthal, Daniel. 1941. “Mathematical Theory of Heat Distribution during Welding and Cutting.” *Welding Journal* 20(5).

Rosenthal, Daniel. 1946. “The Theory of Moving Sources of Heat and Its Application of Metal Treatments.” *Transactions of ASME* 68:849–66.

Santos, Edson Costa, Masanari Shiomi, Kozo Osakada, and Tahar Laoui. 2006. “Rapid Manufacturing of Metal Components by Laser Forming.” *International Journal of Machine Tools and Manufacture* 46(12–13):1459–68.

Scipioni Bertoli, Umberto, Gabe Guss, Sheldon Wu, Manyalibo J. Matthews, and Julie M.

Schoenung. 2017. “In-Situ Characterization of Laser-Powder Interaction and Cooling Rates through High-Speed Imaging of Powder Bed Fusion Additive Manufacturing.” *Materials and Design* 135:385–96. Retrieved (https://doi.org/10.1016/j.matdes.2017.09.044).

Sih, Samuel Sumin and Joel W. Barlow. 2004. “The Prediction of the Emissivity and Thermal Conductivity of Powder Beds.” *Particulate Science and Technology* 22(4):427–40.

Singh, S. S. et al. 2009. “Studies on Laser Sintering of Mechanically Alloyed Al50Ti40Si10 Composite.” *Materials Science and Engineering A* 501(1–2):242–47.

Steen, W. M., J. Dowden, M. Davis, and P. Kapadia. 1988. “A Point and Line Source Model of Laser Keyhole Welding.” *Journal of Physics D: Applied Physics* 21(8):1255–60. Retrieved (http://stacks.iop.org/0022-3727/21/i=8/a=002?key=crossref.4e93e15e72f05d519583e955f2211689).

Steen, William M. and J. Mazumder. 2010. *Laser Material Processing*. Retrieved (http://books.google.com/books?id=gPsq0HHAU4UC&pgis=1).

Trapp, Johannes, Alexander M. Rubenchik, Gabe Guss, and Manyalibo J. Matthews. 2017. “In Situ Absorptivity Measurements of Metallic Powders during Laser Powder-Bed Fusion Additive Manufacturing.” *Applied Materials Today* 9:341–49. Retrieved (http://dx.doi.org/10.1016/j.apmt.2017.08.006).

Vail, Neil K., Badrinarayan Balasubramanian, Joel W. Barlow, and Harris L. Marcus. 1996. “A Thermal Model of Polymer Degradation during Selective Laser Sintering of Polymer Coated Ceramic Powders.” *Rapid Prototyping Journal* 2(3):24–40.

Vishnu, P. Ravi, W. B. Li, and K. E. Easterling. 1991. “Heat Flow Model for Pulsed Welding.” *Materials Science and Technology* 0836(July). Retrieved (http://www.maneyonline.com/doi/abs/10.1179/mst.1991.7.7.649).

Wang, Shuo et al. 2017. “Research on High Layer Thickness Fabricated of 316L by Selective Laser Melting.” *Materials* 10(9).

Xia, Mujian et al. 2017. “Porosity Evolution and Its Thermodynamic Mechanism of Randomly Packed Powder-Bed during Selective Laser Melting of Inconel 718 Alloy.” *International Journal of Machine Tools and Manufacture* 116(November 2016):96–106. Retrieved (http://dx.doi.org/10.1016/j.ijmachtools.2017.01.005).

Yadroitsev, I., Ph Bertrand, and I. Smurov. 2007. “Parametric Analysis of the Selective Laser Melting Process.” *Applied Surface Science* 253(19):8064–69.

Yadroitsev, I., A. Gusarov, I. Yadroitsava, and I. Smurov. 2010. “Single Track Formation in Selective Laser Melting of Metal Powders.” *Journal of Materials Processing Technology* 210(12):1624–31.

Yadroitsev, I., P. Krakhmalev, and I. Yadroitsava. 2015. “Hierarchical Design Principles of Selective Laser Melting for High Quality Metallic Objects.” *Additive Manufacturing* 7:45–56. Retrieved (http://dx.doi.org/10.1016/j.addma.2014.12.007).

Yadroitsev, I., P. Krakhmalev, I. Yadroitsava, S. Johansson, and I. Smurov. 2013. “Energy Input Effect on Morphology and Microstructure of Selective Laser Melting Single Track from Metallic Powder.” *Journal of Materials Processing Technology* 213(4):606–13. Retrieved (http://dx.doi.org/10.1016/j.jmatprotec.2012.11.014).

Yadroitsev, I., I. Shishkovsky, P. Bertrand, and I. Smurov. 2009. “Manufacturing of Fine-Structured 3D Porous Filter Elements by Selective Laser Melting.” *Applied Surface Science* 255(10):5523–27.

Yap, C. Y. et al. 2015. “Review of Selective Laser Melting: Materials and Applications.” *Applied Physics Reviews* 2(4). Retrieved (http://dx.doi.org/10.1063/1.4935926).

Zeng, Kai, Deepankar Pal, and Brent Stucker. 2012. “A Review of Thermal Analysis Methods in Laser Sintering and Selective Laser Melting.” *Proceedings of the Solid Freeform Fabrication Symposium , Austin, TX, August 6-8* 796.

Zhang, Baicheng and Christian Coddet. 2015. “Selective Laser Melting of Iron Powder: Observation of Melting Mechanism and Densification Behavior Via Point-Track-Surface-Part Research.” *Journal of Manufacturing Science and Engineering* 138(5):051001. Retrieved (http://manufacturingscience.asmedigitalcollection.asme.org/article.aspx?doi=10.1115/1.4031366).

9. Appendix A – Integration constants and limits

The integration constants and limits of Vishnu *et al.*'s solution for a pulsed wave Gaussian distributed moving heat source are hereby reported (for the complete derivation of the terms please refer to Vishnu *et al.* [4]):

$$\alpha = \frac{k_p}{\rho_p c_p} \tag{9}$$

$$r_B = \frac{d_0}{2\sqrt{2}} \tag{10}$$

$$t_0 = \frac{r_B^2}{4\alpha_p} \tag{11}$$

$$\xi = x - v(t + t_0) \tag{12}$$

$$M = \frac{z^2}{4\alpha_p t_0} \tag{13}$$

$$N = \frac{\xi^2 + y^2}{4\alpha_p t_0} \tag{14}$$

$$P = \frac{v^2 t_0}{4\alpha_p} \tag{15}$$

Table 8. Integration limit for peak power contribution to the temperature distribution

Integration Limit	$\boldsymbol{t \leq (n-1)t_{tot}}$	$\boldsymbol{(n-1)t_{tot} < t \leq (n-1)t_{tot} + t_{on}}$	$\boldsymbol{t > (n-1)t_{tot} + t_{on}}$
a_n	0	0	$\sqrt{\frac{t - [(n-1)t_{tot} + t_{on}]}{t_0}}$
b_n	0	$\sqrt{\frac{t - (n-1)t_{tot}}{t_0}}$	$\sqrt{\frac{t - (n-1)t_{tot}}{t_0}}$

Table 9. Integration limits for background power contribution to the temperature distribution

Integration Limit	$\boldsymbol{t \leq (n-1)t_{tot} + t_{on}}$	$\boldsymbol{(n-1)t_{tot} + t_{on} < t \leq nt_{tot}}$	$\boldsymbol{t > nt_{tot}}$
a_n	0	0	$\sqrt{\frac{t - nt_{tot}}{t_0}}$
b_n	0	$\sqrt{\frac{t - [(n-1)t_{tot} + t_{on}]}{t_0}}$	$\sqrt{\frac{t - [(n-1)t_{tot} + t_{on}]}{t_0}}$

List of figures

List of tables